ACS Photonics

pubs.acs.org/journal/apchd5

Letter

Vibrational Coupling to Epsilon-Near-Zero Waveguide Modes

Thomas G. Folland,* Guanyu Lu, Autumn Bruncz, J. Ryan Nolen, Marko Tadjer, and Joshua D. Caldwell*

Cite This: *ACS Photonics* 2020, 7, 614–621

Read Online

ACCESS | Metrics & More | Article Recommendations | Supporting Information

ABSTRACT: Epsilon near zero modes offer extreme field enhancement that can be utilized for developing enhanced sensing schemes. However, demonstrations of enhanced spectroscopies have largely exploited surface polaritons, mostly due to the challenges of coupling a vibrational transition to volume-confined epsilon near zero modes. Here we fabricate high aspect ratio gratings (up to 24.8 μm height with greater than 5 μm pitch) of 4H-SiC, with resonant modes that couple to transverse magnetic and transverse electric incident fields. These correspond to metal−insulator−metal waveguide modes propagating downward into the substrate. The cavity formed by the finite length of the waveguide allows for strong absorption of incident infrared light (>80%) with Q factors in excess of 90, including an epsilon near zero waveguide mode with ε_{eff} = 0.0574 + 0.008i. The localization of the electromagnetic fields within the gap between the grating teeth suggests an opportunity to realize a new platform for studying vibrational coupling in liquid environments, with potential opportunities for enhanced spectroscopies. We show that these modes are supported in anhydrous and aqueous environments and that high aspect ratio gratings coherently couple to the vibrational transition in the surrounding liquid.

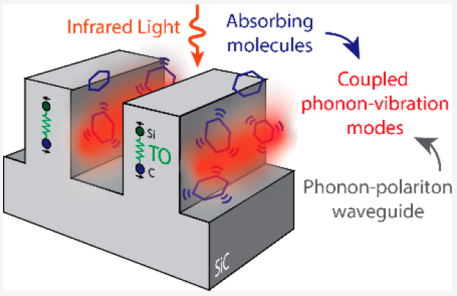

KEYWORDS: *phonon polariton, surface-enhanced spectroscopy, infrared spectroscopy, grating*

Downloaded via VANDERBILT UNIV on May 29, 2020 at 19:24:13 (UTC).
See https://pubs.acs.org/sharingguidelines for options on how to legitimately share published articles.

The electromagnetic field confinement offered by surface polaritons[1,2] and epsilon-near-zero (ENZ)[3−7] modes have long been discussed for applications in surface-enhanced sensing[8−13] and vibrational coupling.[14,15] While surface plasmon polaritons (SPPs) have been extensively explored, demonstrating enhanced spectroscopies using ENZ modes has remained challenging. This is largely because at optical frequencies ENZ modes are often realized by coupling light into a material where epsilon is close to zero[16−18] or via waveguides that are not hollow and therefore incompatible with confining the analyte of interest within the region of highly confined electromagnetic fields.[3,4] In this Letter, we investigate high-aspect-ratio grating (HAG) structures designed to support surface phonon polaritons (SPhPs)[1] at the interface between the polar crystal grating surfaces and the surrounding environment.[19] We show that the modes supported by this structure behave like metal−insulator−metal (MIM) waveguide modes in a short cavity.[20−22] Furthermore, due to this architecture, these structures support an ENZ mode in the gap between the grating teeth. This enables the first colocation of strongly confined ENZ fields with an analyte of interest, including liquids, with a large mode overlap. As proof of this, we demonstrate that the ENZ fields can coherently couple to vibrational transitions in a liquid. Thus, this constitutes a platform for studying ENZ and SPhP strong coupling at infrared (IR) frequencies, with potential applications in surface-enhanced spectroscopies[8−13,23] as well as light-controlled chemistry.[14,15]

This study exploits high aspect ratio gratings, which have a height (h) that is much larger than their period (Λ; see Figure 1a). In HAGs and high aspect nanopillars, surface polariton modes are supported between the teeth, propagating as MIM waveguide modes downward into the grating.[20−22,24,25] The frequency of the modes can be controlled by changing the effective index of refraction (n_{eff}) of the polariton wave using the size of the air gap (g) between the teeth or the height of the grating (h, see Figure 1b−d). Furthermore, polaritonic modes in these structures have been demonstrated to improve sensitivity for surface-enhanced Raman (SERS) and solid-phase IR sensing.[26,27] Existing studies have focused on transverse magnetic (TM) waveguide modes in materials supporting surface plasmons, as opposed to the transverse electric (TE) waveguide modes that can support ENZ-type behavior. In our work, we leverage SPhPs in 4H-SiC, which can be supported within the spectral region between ∼792 and 972 cm^{-1}. This spectral region is referred to as the Reststrahlen band and is bound by the transverse (TO) and longitudinal optic (LO) phonons of the material.[28] The low scattering

Received: January 15, 2020
Published: February 26, 2020

© 2020 American Chemical Society

https://dx.doi.org/10.1021/acsphotonics.0c00071
ACS Photonics 2020, 7, 614–621

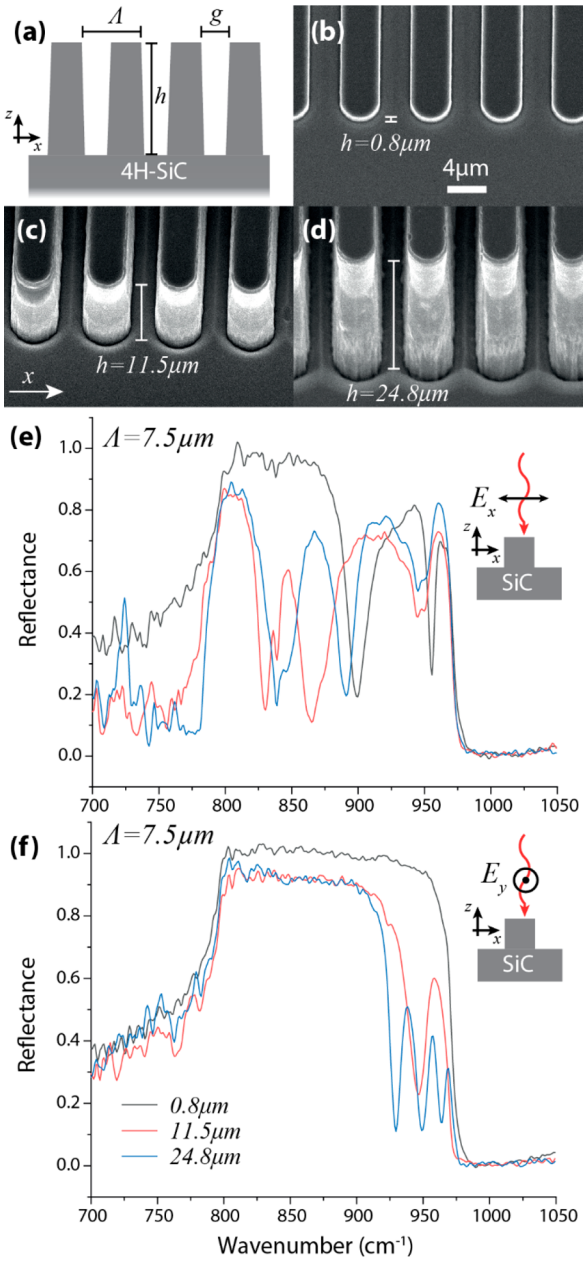

Figure 1. Schematic (a) and scanning electron microscope (SEM) images of deep-etched SiC grating structures (b–d) illustrate the significant variation in etch depths (h = 0.85, 11, and 24.8 μm, respectively) of three grating structures with Λ = 7.5 μm and t = 4 μm, as viewed in an electron microscope at 30° off normal. Polarized FTIR spectra with an electric field in (e) TM or (f) TE orientation.

losses associated with polar optic phonons,[19,29] grating,[30−32] and nanoantenna[28,33−36] structures can support resonances with high Q factors, with a maximum reported of ~300[28,33] and 400 for far-field and near-field[37] measurements, respectively. This makes them an ideal system for studies of ENZ materials and enhanced spectroscopic methods.

Despite the impressive properties of SPhPs, there have been limited demonstrations of these modes for realizing effects such as surface-enhanced infrared absorption (SEIRA)[8−13,23] spectroscopy, especially on nonsolid analytes.[38] This is largely due to the challenges of coupling to the highly localized fields supported by SPhP resonators in a liquid environment, where infrared light is generally strongly attenuated. The waveguide modes in HAGs discussed here overcome this problem, as the optical fields are strongly localized within the gaps between grating teeth. One of the remarkable properties of the HAG structures studied in this work is that their resonant modes couple to both TM and TE incident fields.[39] While TM incident fields form confined MIM polaritonic modes (with n_{eff} > 1, as in past work[30−32]), the TE-coupled modes exhibit behavior similar to the near-cutoff frequency of waveguides,[3−6] showing n_{eff}< 1. Here, we provide a complete analytical model for these TE modes and demonstrate that they can be attributed to standing waves in a finite length MIM grating. This allows us to demonstrate that the lowest-order TE mode can be classed as an ENZ waveguide mode, with an ε_{eff} = 0.0574 + 0.008i. In order to explore the possibility of leveraging these ENZ modes for liquid-based sensing, we study the properties of the resonant modes in various working liquids, including water and alcohols. We find that the MIM modes are supported in anhydrous environments and can also be observed in aqueous environments, but are attenuated and broadened in the latter. We then use mixtures of different solvents to study the possibility of surface-enhanced sensing and strong coupling within these structures. We show that waveguide modes in HAG gratings can couple to vibrational transitions in the liquid, resulting in mode splitting, indicative of coherent coupling, with a splitting of up to 7.8 cm^{-1} about the ENZ resonant frequency. Our results illustrate that HAG structures provide a platform for studying vibrational coupling between SPhPs and vibrational bands in the IR[14,15,40−42] and constitutes the first implementation of ENZ modes for coupling to vibrational bands in liquids.

Gratings with a pitch (Λ) ranging from 5 to 10 μm and grating tooth spacings (g; see Figure 1a–d) such that a constant fill fraction (g/Λ) of 0.5 is maintained and were fabricated using a combination of photolithography and deep-reactive ion etching (see Methods). Three different etch depths (Figure 1b–d) were used, and the samples were characterized using FTIR microspectroscopy (see Methods). The shallow grating structures (0.8 μm) exhibit a series of SPhP grating modes when reflection is collected in TM polarization (incident field oriented along E_x), as shown in Figure 1e, and explored in past works.[30,31] However, no discernible modes were observed in TE polarization (field was oriented along E_y), as anticipated for a grating featuring a subdiffractional pitch (Figure 1f). For deep structures (11.5 and 24.8 μm), TM polarization also resulted in the excitation of SPhP modes, albeit with additional absorption bands. Interestingly, the TE-polarized reflection spectra of these deep-etched gratings also exhibit strong resonant response, with a series of sharp absorption peaks observed throughout the SiC Reststrahlen band (Figure 1). In contrast, as shown in the shallow gratings, TE polarized light cannot directly excite SPhP modes, while the narrow grating pitch prevents in-coupling via diffractive orders with normal incidence light. Thus, the modes in our HAG structures must be derived from waveguide-like modes, which are known to be supported in MIM structures.[4,6] In this way, our grating is behaving like a closely packed array of short waveguides that light can propagate into from free space, similar to coupling in and out of an optical fiber. While the SiC gratings discussed here do not contain any metal, the negative permittivity of the SiC within the Reststrahlen band provides the metallic behavior necessary for the MIM design. Numerical simulations of the grating spectra support this ascertion, as shown in Supporting Information, section 1, and

https://dx.doi.org/10.1021/acsphotonics.0c00071
ACS Photonics 2020, 7, 614−621

Figure S1. Both TE and TM field profiles illustrate electromagnetic fields confined within the gap between the grating "teeth", with a series of standing waves in the cavity. The localization of the electromagnetic fields within the teeth is ideal for enhanced spectroscopic applications, as the air gaps can be filled with a material for analysis. Furthermore, the TE waves have a longer wavelength than light in free space, which suggests an extremely low refractive index and, hence, an indication of ENZ behavior.

To provide a complete description of the TE-polarized waveguide modes and their ENZ properties, we can study the pitch dependence of the modes (Figure 2a) and compare to a simple analytical model for a cavity formed in a short waveguide (Figure 2b,c). The narrowest pitch structure supports modes located at the high-frequency edge of the Reststrahlen band. As the grating pitch is increased, the modes continuously red-shift and additional modes appear. This is consistent with a continuous tuning in the dispersion of the waveguide modes as the gaps between the SiC teeth increase. To demonstrate this, we use a simple slab waveguide model to calculate the dispersion of the TE-polarized waveguide modes (inset Figure 2b), employing the standard MIM waveguide equations for symmetric and antisymmetric modes;[6]

$$k_2 + k_1 \tanh\left(\frac{-ik_1 g}{2}\right) = 0 \quad (1)$$

$$k_2 + k_1 \coth\left(\frac{-ik_1 g}{2}\right) = 0 \quad (2)$$

Here, g is the thickness of the gap, $k_i^2 = \varepsilon_i k_0^2 - \beta^2$, ε_i is the dielectric function of each layer (1 = air, 2 = SiC), k_0 is the free-space wavevector, and β is the guided wavevector. Instead of plotting the waveguide propagation constant β, we choose to plot the effective index of the wave ($n_{\text{eff}} = \beta/k_0$), as shown in Figure 2b. We highlight that this effective index is not due to any kind of effective medium approximation but, instead, describes light in an isolated MIM waveguide. We find that the cutoff frequency of the TE waveguide mode (where n_{eff} goes to zero) varies dramatically as the pitch is increased, exhibiting a significant red-shift, consistent with our experimental data. Furthermore, to more accurately compare to our experimentally measured modal frequencies, we can also express a cavity resonance condition in terms of n_{eff}.[24] This condition will state at which values of n_{eff} the cavity wave is supported in the continuous dispersion spectrum for a given cavity length. The fields of Figure S1 suggest that the waveguide forms a closed cavity from which we can write the closed cavity condition:

$$n_{\text{eff}} = \frac{l\lambda}{2h} \quad (3)$$

where l is the mode order, λ is the free-space wavelength, and h is the grating height. The cavity condition is plotted in Figure 2b using dashed lines. The points where the cavity condition (dashed) and waveguide dispersion (solid) lines intersect indicate where we would anticipate experimentally measured modes (symbols). In general, the experimental modal positions qualitatively agree with the trends and rough spectral shape. Deviations in the mode frequencies are likely due to two effects, lateral coupling between different waveguide teeth (evident by examining fields presented in Figure S1) and tapering of the waveguide width, that occurred due to the RIE processing, neither of which is considered in the analytical

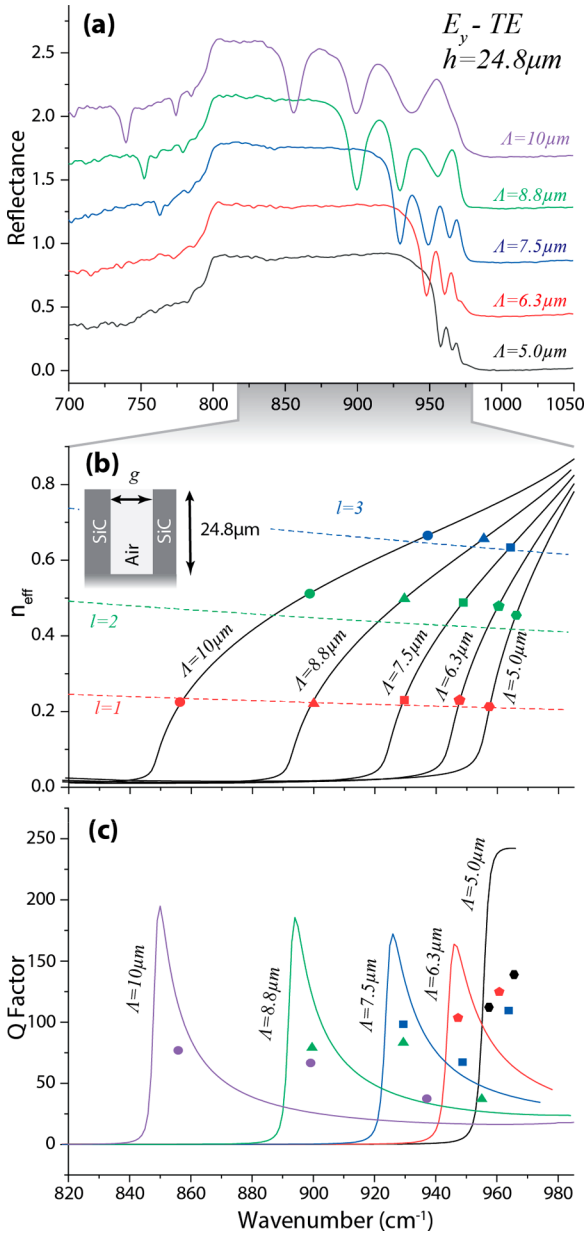

Figure 2. Pitch tuning of TE type waveguide modes in deep SiC gratings, (a) experimentally measured by FTIR spectroscopy. The absorption below the TO phonon frequency is due to high index modes forming in the SiC teeth. (b) Analytical mode solutions for the waveguide (model inset). Mode positions of standing waves formed by the TE waveguide modes can be found from the crossing of the waveguide dispersion (solid lines) and the cavity resonance condition (dashed lines, colored). The experimentally measured mode positions are overlaid on top of the analytical dispersion curves in (b), with circles, triangles, squares, pentagons, and hexagons representing modes in 10, 8.8, 7.5, 6.3, and 5.0 μm gratings, respectively. (c) Analytically calculated Q factor compared against the experimentally measured Q factors, with the same shapes as (b).

model. However, this simple model does provide validation that these resonances can be attributed to TE-type waveguide modes, with $n_{\text{eff}} < 1$, and demonstrates that a simple model can be used to estimate the mode frequencies for a simplified design process. We note that the $l = 1$ mode possesses an extremely low effective mode index of 0.235, which equates to an effective permittivity of $\varepsilon_{\text{eff}} = 0.0574 + 0.008i$. As this is a

https://dx.doi.org/10.1021/acsphotonics.0c00071
ACS Photonics 2020, 7, 614−621

comparable permittivity to exemplary ENZ materials, including doped CdO[16] ($\varepsilon_{eff} \sim 0 + 0.4i$) and AlN[17] ($\varepsilon_{eff} \sim 0 + 0.05i$), the waveguide mode at the heart of this work can also be considered an ENZ waveguide mode.

This same cavity model can also be used to estimate the modal Q factors associated with these frequencies. We can write the Q factor as

$$Q = \frac{\tau\omega}{2} \tag{4}$$

where τ is the modal lifetime and ω is the frequency of the mode. The total mode lifetime is related to the rate at which light escapes from the cavity on each round trip ($1/\tau_c$), as well as the rate at which light is absorbed into the silicon carbide within the MIM mode ($1/\tau_s$):[43]

$$\frac{1}{\tau} = \frac{1}{\tau_c} + \frac{1}{\tau_s} = v_g\left(\frac{\ln(R)}{2h} + \mathrm{Im}(\beta)\right) \tag{5}$$

where v_g is the group velocity of the mode (calculated from the dispersion) and R is the power reflection coefficient at the top of the cavity. In general, the value of R is given by the coupling between waveguide modes and multiple diffractive orders in free space.[44] However, as the spacing between the waveguides is below the diffraction limit at normal incidence, removing coupling to diffractive modes, we can estimate R using the conventional Fresnel formula; $R = ((n_{eff} - 1)/(n_{eff} + 1))^2$. The calculated Q factor shows a sharp increase close to the cutoff frequency of the mode, as shown in Figure 2c, attributed to the high cavity reflection as n_{eff} and ε_{eff} approach zero. The cavity reflection drops off rapidly away from this frequency, and this limits our modal lifetime at higher frequencies (see Supporting Information, Figure S2). The experimentally measured Q values are similar to those predicted by the model, but we find the analytical model overestimates Q for the $l = 1$ mode, and underestimates it for $l = 2$ and 3. This is again likely due to the nonvertical sidewalls in our structures, which will modify the dispersion of Figure 2b and, hence, change the MIM mode group velocity on which the calculated Q is directly dependent. However, the similarities between experimentally measured and analytically predicted Qs provides further evidence that these modes can be seen as standing waves in a finite length MIM waveguide. These trends are also observable in the intermediate aspect ratio ($h = 11.5$ μm) gratings, as shown in Supporting Information, Figure S3.

Given the ability of such structures to create resonant cavity modes (including an ENZ mode), we can now turn our attention to their application for liquid sensing. In particular, the Reststrahlen band of SiC lines up with the frequencies of many volatile organic compounds, where high sensitivity sensing is of distinct interest.[23] To study the potential for using HAG gratings in liquid sensing applications, we first study their mode spectra in liquid environments. To achieve this, we placed the grating samples inside a liquid cell (see Methods), compatible with the FTIR spectrometer (Figure 3a), to probe the response in the presence of a liquid (water and acetone). We measured the IR reflectance spectrum from the grating structures (Figure 3b), as well as from the unpatterned surrounding substrate, to the side of the gratings, which provides a "reference" measurement of the strength and frequency for a film of liquid with the same thickness (t) as the grating height $t \sim h$. A cavity effect is also present in this reference measurement, formed by reflections between SiC and the BaF_2 coverslip, resulting in interference dips in the spectrum (as seen at 940 cm^{-1} for air in Figure 3 and, more clearly, at other frequencies in Figure S11). For acetone, the vibrational band occurs at ~900 cm^{-1}, whereas for water, light is generally attenuated across the complete Reststrahlen band of SiC. When submerged in acetone, the grating exhibits two additional waveguide modes, which can be attributed to the higher index of the surrounding medium modifying the waveguide dispersion. However, the modes have a similar Q factor and absorption to the grating in air. In water, the grating spectrum is heavily attenuated, but has enhanced transmission versus the spectrum taken through liquid alone. This is likely due to the localization of the electromagnetic fields inside the silicon carbide, which reduces loss from the liquid. These results demonstrate that HAG structures are compatible with liquid-based sensing approaches, and in Supporting Information, section 4, we show that the frequency tuning is comparable to past demonstrations of liquid sensing.[8]

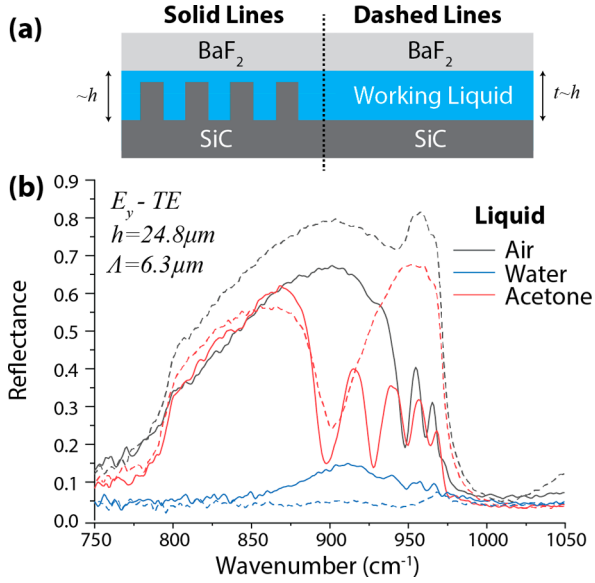

Figure 3. Response of TE waveguide modes in a liquid environment (a) shows a schematic of the experimental configuration and (b) mode spectrum of the HAG inside a liquid cell filled with air, water, and acetone.

To investigate the possibility of using HAGs and ENZ modes as a platform for vibrational sensing and strong coupling, we also studied the behavior of polaritonic resonances in mixtures of a range of different solvents, including acetone, IPA, toluene, and cyclohexane, all of which have some degree of vibrational activity within the SiC Reststrahlen band (see Figure S5). As cyclohexane exhibits a relatively strong (absorption coefficient estimated at 334 cm^{-1}), sharp absorption band (CH_2 rocking) located at the center of the Reststrahlen region (903 cm^{-1}), which makes it ideal for such studies. In these studies, we focus on the TE-type modes, as the mode spectrum for these structures is significantly simpler.

In order to tune the cavity mode to the frequency of the cyclohexane vibration, we study a range of different gratings with slightly different pitches, as shown in Figure 4a. We find that a grating with a $\Lambda = 6.48$ μm results in an ENZ waveguide mode with strong spectral overlap with the vibrational mode of the neat cyclohexane that it is immersed in. The interaction between these two resonant modes results in a modal splitting,

https://dx.doi.org/10.1021/acsphotonics.0c00071
ACS Photonics 2020, 7, 614−621

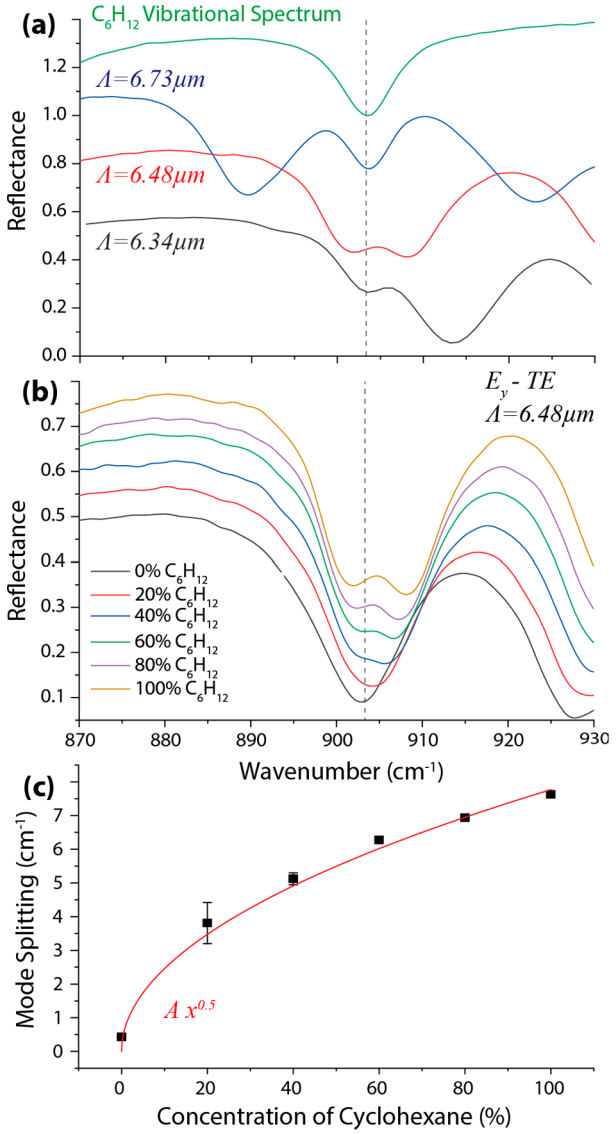

Figure 4. Strong coupling between a waveguide mode and the vibrational mode of cyclohexane. (a) This is how the grating pitch can be controlled in order to overlap the cavity mode with the vibrational mode, producing mode splitting. (b) Concentration-dependent mode splitting in HAG modes. (c) Concentration-dependent mode splitting in the vibrational cavity.

which is indicative of coherent coupling.[14,41,42] In order to verify that this can be attributed to coherent coupling, we dilute the cyclohexane and study how the modal splitting changes with modified molecular concentration. However, to ensure that the cavity mode of the ENZ waveguide is not spectrally shifted away from the vibrational resonance, a solvent with a similar refractive index as cyclohexane must be used. We find that a 1:1 mixture of IPA and toluene serves as an acceptable solvent, as it maintains the cavity resonance frequency close to the 903 cm^{-1} vibrational band of cyclohexane (see Figure S6). Varying the concentration of cyclohexane in this solvent mixture demonstrates a tunable splitting between the waveguide mode and the vibrational transition (Figure 4b). By fitting the data in Figure 4b, we show that the mode splitting follows the simple $\sqrt{N}$ dependence on the concentration of molecules (Figure 4c),[14] providing further evidence of vibrational coherent coupling. The maximum mode splitting is 7.8 cm^{-1}, which is comparable to the full width at half maximum of the uncoupled cyclohexane vibrational resonance (7.9 cm^{-1}) and the cavity mode (14.5 cm^{-1}), placing the observed splitting close to the threshold of strong coupling. By implementing a crude dielectric function that would be analogous to cyclohexane, we see that this result is also consistent with our analytical model (see Figure S7). We note that the coupling strength is largely limited by the relatively weak absorption of the cyclohexane vibrational band (334 cm^{-1}) when compared with vibrational bands used in past works on vibrational coupling (exceeding 3500 cm^{-1}).[42] We note that, while IPA could in principle be used as an excellent target molecule, as it possesses a very strong absorption band at 952 cm^{-1}, with α = 3300 cm^{-1}. However, in practice, the vibrational energy of the mode is too close to the edge of the Reststrahlen band, as shown in Supporting Information, Figures S8–S10, and as a result, the mode is only broadened. This highlights the importance of using the l = 1 ENZ mode (which exhibits the largest Q) for such strong coupling experiments.

In summary, we have fabricated HAGs made of 4H-SiC, which supports both TE- and TM-polarized SPhP waveguide modes in the long-wave IR. Unlike the response from a shallow grating, where modes propagate along the surface of the grating teeth, in HAG structures the modes propagate vertically downward into the substrate. These waveguide modes are generally described by simple MIM waveguide equations, and strongly localize light in between the grating teeth. For TM modes, this is associated with polaritonic confinement effects, however for TE modes this is associated with a reduction in the effective mode index to values less than 1. Due to the finite height of the grating, the modes formed in the gratings take the form of standing-wave-type cavity modes, with the lowest order resonance behaving as an ENZ waveguide mode. The frequency of the modes is generally described by a combination of the waveguide dispersion and a cavity resonance condition. We go on to show that these modes can be supported in liquid environments, finding that, while SPhP modes are readily supported in anhydrous environments, they are heavily attenuated in aqueous environments. Finally, we show that these gratings can support vibrational coherent coupling between the ENZ mode and the vibrational band in cyclohexane. This constitutes the first implementation of ENZ modes for enhanced spectroscopy, as well as the formation of a hybrid phonon-vibration polariton mode.

METHODS

Device Fabrication. Gratings with a pitch (Λ) ranging from 5 to 10 μm and grating tooth spacing (g; see Figure 1) with a constant fill fraction (g/Λ) of 0.5 were fabricated using a combination of photolithography and inductively coupled plasma (ICP) process. Specifically, an on-axis, undoped 4H-SiC wafer was cleaned in piranha solution, followed by a DI rinse and N_2 blow dry. The wafer was seeded by Cr/Au (100 Å/1000 Å) deposited using electron-beam evaporation, patterned using contact photolithography, and selectively electroplated with a Ni etch mask (1.7 μm thick). Dry etching was carried out following the processes developed in ref 45. Following etching, the metal mask was removed in aqua regia for 1 h, followed by 60 s in chrome etchant and a DI rinse. We show scanning electron images of the fabricated grating structures with Λ = 7.5 μm and g = 3.5 μm in Figure 1b–e

https://dx.doi.org/10.1021/acsphotonics.0c00071
ACS Photonics 2020, 7, 614–621

with three different etch depths; 0.8, 11, and 24 μm. These depths were obtained using a 7 min β3-etch (1:9 SF_6:O_2, 50 sccm total flow), a 60 min modified β-etch with SF_6:O_2 ratio reduced to 1:6 for better mask selectivity, and a 60 min standard α etch with 10:1 SF_6:O_2 ratio, respectively. Measurements of the profile of all gratings studied show an average sidewall angle of approximately 2.3° ± 1.2°.

Optical Characterization. Reflectance spectra for the grating structures were measured using a Bruker Hyperion 2000 IR Microscope coupled to a Bruker Vertex 70v Fourier transform IR spectrometer (FTIR) using a spectral resolution of 2 cm^{-1}. The microscope is equipped with a refractive Ge objective (5×, NA = 0.17, Pike Technologies), a Ge wire grid polarizer (Pike Technologies) and liquid-nitrogen-cooled mercury cadmium telluride (MCT) detector. The use of a 5× objective removes out-of-plane electromagnetic field components from the incident field, which simplifies the analysis of our initial results. It also ensures that all of the structures studied are well-below the diffraction limit (removing conventional diffractive effects).

Numerical Simulations. Simulations were performed in CST studio suite 2018, where the SiC grating structure uses a single grating period and unit cell boundary conditions, and a perfectly matched layer for the substrate. The dielectric function used for 4H-SiC was derived from that presented in ref 46. In all of our analyses, we define the periodic axis of the grating as the x-axis and the etch direction as the z-axis (see Figure 1.)

Liquid-Based Experiments. Liquid experiments were performed in a Pike Technologies demountable liquid cell using BaF_2 windows. To use the liquid cell with our small (1 cm by 1 cm by 500 μm) samples, a 0.02' (508 μm) Teflon spacer was used in the cell. Two samples could be loaded in the cell simultaneously, allowing an accurate comparison between experimental results on different devices. The cell was loaded through a drilled BaF_2 window using a syringe, and the liquid was changed by drying the liquid cell using dry nitrogen. The Teflon spacer was not the exact thickness of the SiC wafer, but by examining the fringes formed by the BaF_2-air-SiC cavity outside the Reststrahlen band when an FTIR spectrum is taken next to the grating (see Supporting Information, Figure S11), we can estimate the spacing between the cover and the sample. The frequency spacing of the fringes (Δf) 673 cm^{-1} (197 cm^{-1}), for h = 0.8 μm (h = 24.8 μm) gratings is related to the size (L) of the cavity by $L = c/(2n\Delta f)$, where c is the speed of light and n is the index of the medium. This gives a height of the control cavity of 7.4 μm for the grating with h = 0.8 μm and 25.4 μm for the grating with h = 24.8 μm, suggesting that the cell provides a gap of a few microns between the top of the grating and the BaF_2 cover.

■ ASSOCIATED CONTENT

Supporting Information

The Supporting Information is available free of charge at https://pubs.acs.org/doi/10.1021/acsphotonics.0c00071.

Figure S1: Finite element simulations of grating response and field profile. Figure S2: Mode lifetime for TE Waveguide modes. Figure S3: Mode spectrum for h = 11.5 μm grating. Figure S4: Influence of liquid environment on grating resonances. Figure S5: Infrared spectra of solvents. Figure S6: Mode tuning in solvent mixtures. Figure S7: Analytical analysis of coherent coupling in the waveguide. Figure S8: Study of acetone−IPA mixtures. Figure S9: Coupling in acetone−IPA mixtures. Figure S10: Dielectric function for acetone−IPA mixtures. Figure S11: Fabry−Perot interference for cavity size (PDF)

■ AUTHOR INFORMATION

Corresponding Authors

Joshua D. Caldwell − *Department of Mechanical Engineering, Vanderbilt University, Nashville, Tennessee 37212, United States;* orcid.org/0000-0003-0374-2168; Email: josh.caldwell@vanderbilt.edu

Thomas G. Folland − *Department of Mechanical Engineering, Vanderbilt University, Nashville, Tennessee 37212, United States;* orcid.org/0000-0002-4665-235X; Email: thomas.g.folland@vanderbilt.edu

Authors

Guanyu Lu − *Department of Mechanical Engineering, Vanderbilt University, Nashville, Tennessee 37212, United States;* orcid.org/0000-0001-8960-0464

Autumn Bruncz − *Department of Mechanical Engineering, Vanderbilt University, Nashville, Tennessee 37212, United States; Department of Physics, University of Alabama in Huntsville, Huntsville, Alabama 35899, United States*

J. Ryan Nolen − *Interdisciplinary Materials Science, Vanderbilt University, Nashville, Tennessee 37212, United States*

Marko Tadjer − *U.S. Naval Research Laboratory, Washington, D.C. 20375, United States*

Complete contact information is available at: https://pubs.acs.org/10.1021/acsphotonics.0c00071

Author Contributions

The manuscript was written through contributions of all authors. T.G.F. and J.D.C. conceived of the experiment. Samples were prepared by M.T., and characterized by T.G.F. and J.R.N., and A.B., T.G.F., and G.L. performed numerical simulations and analytical calculations. All authors have given approval to the final version of the manuscript.

Funding

Support for J.DC., T.G.F., and J.R.N. was partially provided by the Office of Naval Research under Contract Number N00014-18-1-2107. J.R.N, T.G.F., and J.D.C. also acknowledge support from the Vanderbilt School of Engineering through the latter's startup funding package. A.B. acknowledges support from the Vanderbilt University VUSE summer internship program. Work at the Naval Research Laboratory is supported by the Office of Naval Research.

Notes

The authors declare no competing financial interest.

■ ACKNOWLEDGMENTS

We would like to thank Mr. Milton Rebbert for additional sample processing at NRL. We would also like to thank the Vanderbilt Institute of Nanoscale Science and Engineering for access to scanning electron microscopy.

■ REFERENCES

(1) Folland, T. G.; Nordin, L.; Wasserman, D.; Caldwell, J. D. Probing polaritons in the mid- to far-infrared. *J. Appl. Phys.* **2019**, *125* (19), 191102.

(2) Maier, S. A. *Plasmonics: Fundamentals and Applications*; Springer: Berlin, 2007.
(3) Vesseur, E. J. R.; Coenen, T.; Caglayan, H.; Engheta, N.; Polman, A. Experimental verification of n = 0 structures for visible light. *Phys. Rev. Lett.* **2013**, *110*, No. 013902.
(4) Liu, R.; Roberts, C. M.; Zhong, Y.; Podolskiy, V. A.; Wasserman, D. Epsilon-Near-Zero Photonics Wires. *ACS Photonics* **2016**, *3* (6), 1045−1052.
(5) Alù, A.; Engheta, N. Dielectric sensing in ϵ-near-zero narrow waveguide channels. *Phys. Rev. B: Condens. Matter Mater. Phys.* **2008**, *78* (4), No. 045102.
(6) Dionne, J. A.; Sweatlock, L. A.; Atwater, H. A.; Polman, A. Plasmon slot waveguides: Towards chip-scale propagation with subwavelength-scale localization. *Phys. Rev. B: Condens. Matter Mater. Phys.* **2006**, *73* (3), No. 035407.
(7) Liberal, I.; Engheta, N. The rise of near-zero-index technologies. *Science* **2017**, *358* (6370), 1540.
(8) Neuner, B.; Korobkin, D.; Fietz, C.; Carole, D.; Ferro, G.; Shvets, G. Midinfrared Index Sensing of pL-Scale Analytes Based on Surface Phonon Polaritons in Silicon Carbide. *J. Phys. Chem. C* **2010**, *114* (16), 7489−7491.
(9) Maß, T. W. W.; Taubner, T. Incident Angle-Tuning of Infrared Antenna Array Resonances for Molecular Sensing. *ACS Photonics* **2015**, *2* (10), 1498−1504.
(10) Yoo, D.; Mohr, D. A.; Vidal-Codina, F.; John-Herpin, A.; Jo, M.; Kim, S.; Matson, J.; Caldwell, J. D.; Jeon, H.; Nguyen, N.-C.; Martin-Moreno, L.; Peraire, J.; Altug, H.; Oh, S.-H. High-Contrast Infrared Absorption Spectroscopy via Mass-Produced Coaxial Zero-Mode Resonators with Sub-10 nm Gaps. *Nano Lett.* **2018**, *18* (3), 1930−1936.
(11) Autore, M.; Li, P.; Dolado, I.; Alfaro-Mozaz, F. J.; Esteban, R.; Atxabal, A.; Casanova, F.; Hueso, L. E.; Alonso-González, P.; Aizpurua, J.; Nikitin, A. Y.; Vélez, S.; Hillenbrand, R. Boron nitride nanoresonators for phonon-enhanced molecular vibrational spectroscopy at the strong coupling limit. *Light: Sci. Appl.* **2018**, *7*, 17172.
(12) Berte, R.; Gubbin, C. R.; Wheeler, V. D.; Giles, A. J.; Giannini, V.; Maier, S. A.; De Liberato, S.; Caldwell, J. D. Sub-nanometer Thin Oxide Film Sensing with Localized Surface Phonon Polaritons. *ACS Photonics* **2018**, *5* (7), 2807−2815.
(13) Adato, R.; Yanik, A. A.; Amsden, J. J.; Kaplan, D. L.; Omenetto, F. G.; Hong, M. K.; Erramilli, S.; Altug, H. Ultra-sensitive vibrational spectroscopy of protein monolayers with plasmonic nanoantenna arrays. *Proc. Natl. Acad. Sci. U. S. A.* **2009**, *106* (46), 19227−19232.
(14) Ebbesen, T. W. Hybrid Light−Matter States in a Molecular and Material Science Perspective. *Acc. Chem. Res.* **2016**, *49* (11), 2403−2412.
(15) Herrera, F.; Owrutsky, J. Molecular polaritons for controlling chemistry with quantum optics. *arXiv preprint arXiv:1911.05017* **2019**, na.
(16) Runnerstrom, E. L.; Kelley, K. P.; Folland, T. G.; Nolen, J. R.; Engheta, N.; Caldwell, J. D.; Maria, J.-P. Polaritonic Hybrid-Epsilon-near-Zero Modes: Beating the Plasmonic Confinement vs Propagation-Length Trade-Off with Doped Cadmium Oxide Bilayers. *Nano Lett.* **2019**, *19* (2), 948−957.
(17) Passler, N. C.; Gubbin, C. R.; Folland, T. G.; Razdolski, I.; Katzer, D. S.; Storm, D. F.; Wolf, M.; De Liberato, S.; Caldwell, J. D.; Paarmann, A. Strong Coupling of Epsilon-Near-Zero Phonon Polaritons in Polar Dielectric Heterostructures. *Nano Lett.* **2018**, *18* (7), 4285−4292.
(18) Campione, S.; Brener, I.; Marquier, F. Theory of epsilon-near-zero modes in ultrathin films. *Phys. Rev. B: Condens. Matter Mater. Phys.* **2015**, *91*, 121408.
(19) Caldwell, J. D.; Lindsay, L.; Giannini, V.; Vurgaftman, I.; Reinecke, T.; Maier, S. A.; Glembocki, O. J. Low-Loss, Infrared and Terahertz Nanophotonics with Surface Phonon Polaritons. *Nanophotonics* **2015**, *4*, 44−68.
(20) Sobnack, M. B.; Tan, W. C.; Wanstall, N. P.; Preist, T. W.; Sambles, J. R. Stationary Surface Plasmons on a Zero-Order Metal Grating. *Phys. Rev. Lett.* **1998**, *80* (25), 5667−5670.
(21) Kreiter, M.; Mittler, S.; Knoll, W.; Sambles, J. R. Surface plasmon-related resonances on deep and asymmetric gold gratings. *Phys. Rev. B: Condens. Matter Mater. Phys.* **2002**, *65* (12), 125415.
(22) Liao, Y.-L.; Zhao, Y. Ultrabroadband absorber using a deep metallic grating with narrow slits. *Opt. Commun.* **2015**, *334*, 328−331.
(23) Lu, R.; Li, W.-W.; Mizaikoff, B.; Katzir, A.; Raichlin, Y.; Sheng, G.-P.; Yu, H.-Q. High-sensitivity infrared attenuated total reflectance sensors for in situ multicomponent detection of volatile organic compounds in water. *Nat. Protoc.* **2016**, *11*, 377.
(24) Lyvers, D. P.; Moon, J.-M.; Kildishev, A. V.; Shalaev, V. M.; Wei, A. Gold Nanorod Arrays as Plasmonic Cavity Resonators. *ACS Nano* **2008**, *2* (12), 2569−2576.
(25) Shukla, S.; Kim, K.-T.; Baev, A.; Yoon, Y. K.; Litchinitser, N. M.; Prasad, P. N. Fabrication and Characterization of Gold−Polymer Nanocomposite Plasmonic Nanoarrays in a Porous Alumina Template. *ACS Nano* **2010**, *4* (4), 2249−2255.
(26) Shkondin, E.; Repän, T.; Aryaee Panah, M. E.; Lavrinenko, A. V.; Takayama, O. High Aspect Ratio Plasmonic Nanotrench Structures with Large Active Surface Area for Label-Free Mid-Infrared Molecular Absorption Sensing. *ACS Applied Nano Materials* **2018**, *1* (3), 1212−1218.
(27) Wei, W.; Chen, K.; Ge, G. Strongly Coupled Nanorod Vertical Arrays for Plasmonic Sensing. *Adv. Mater.* **2013**, *25* (28), 3863−3868.
(28) Caldwell, J. D.; Kretinin, A. V.; Chen, Y.; Giannini, V.; Fogler, M. M.; Francescato, Y.; Ellis, C. T.; Tischler, J. G.; Woods, C. R.; Giles, A. J.; Hong, M.; Watanabe, K.; Taniguchi, T.; Maier, S. A.; Novoselov, K. S. Sub-diffractional volume-confined polaritons in the natural hyperbolic material hexagonal boron nitride. *Nat. Commun.* **2014**, *5*, 5221.
(29) Foteinopoulou, S.; Devarapu, G. C. R.; Subramania, G. S.; Krishna, S.; Wasserman, D. Phonon-polaritonics: enabling powerful capabilities for infrared photonics. *Nanophotonics* **2019**, *8*, 2129.
(30) Le Gall, J.; Olivier, M.; Greffet, J.-J. Experimental and theoretical study of reflection and coherent thermal emission by a SiC grating supporting a surface-phonon polariton. *Phys. Rev. B: Condens. Matter Mater. Phys.* **1997**, *55* (15), 10105−10114.
(31) Greffet, J.-J.; Carminati, R.; Joulain, K.; Mulet, J. P.; Mainguy, S. P.; Chen, Y. Coherent emission of light by thermal sources. *Nature* **2002**, *416* (6876), 61−64.
(32) Gubbin, C. R.; Martini, F.; Politi, A.; Maier, S. A.; De Liberato, S. Strong and Coherent Coupling between Localized and Propagating Phonon Polaritons. *Phys. Rev. Lett.* **2016**, *116* (24), 246402.
(33) Caldwell, J. D.; Glembocki, O. J.; Francescato, Y.; Sharac, N.; Giannini, V.; Bezares, F. J.; Long, J. P.; Owrutsky, J. C.; Vurgaftman, I.; Tischler, J. G.; Wheeler, V. D.; Bassim, N. D.; Shirey, L. M.; Kasica, R.; Maier, S. A. Low-Loss, Extreme Sub-Diffraction Photon Confinement via Silicon Carbide Surface Phonon Polariton Nanopillar Resonators. *Nano Lett.* **2013**, *13* (8), 3690−3697.
(34) Wang, T.; Li, P.; Hauer, B.; Chigrin, D. N.; Taubner, T. Optical properties of single infrared Resonant Circular Microcavities for Surface Phonon Polaritons. *Nano Lett.* **2013**, *13* (11), 5051−5055.
(35) Wang, T.; Li, P.; Chigrin, D. N.; Giles, A. J.; Bezares, F. J.; Glembocki, O. J.; Caldwell, J. D.; Taubner, T. Phonon-Polaritonic Bowtie Nanoantennas: Controlling Infrared Thermal Radiation at the Nanoscale. *ACS Photonics* **2017**, *4* (7), 1753−1760.
(36) Alfaro-Mozaz, F. J.; Alonso-González, P.; Vélez, S.; Dolado, I.; Autore, M.; Mastel, S.; Casanova, F.; Hueso, L. E.; Li, P.; Nikitin, A. Y.; Hillenbrand, R. Nanoimaging of resonating hyperbolic polaritons in linear boron nitride antennas. *Nat. Commun.* **2017**, *8*, 15624−15624.
(37) Tamagnone, M.; Chaudhary, K.; Zhu, A.; Meretska, M.; Li, J.; Edgar, J. H.; Ambrosio, A.; Capasso, F. High quality factor polariton resonators using van der Waals materials. *arXiv preprint arXiv:1905.02177* **2019**, na.
(38) Anderson, M. S. Enhanced Infrared Absorption with Dielectric Nanoparticles. *Appl. Phys. Lett.* **2003**, *83* (14), 2964−2966.
(39) Papadakis, G. T.; Davoyan, A.; Yeh, P.; Atwater, H. A. Mimicking surface polaritons for unpolarized light with high-

https://dx.doi.org/10.1021/acsphotonics.0c00071
ACS Photonics 2020, 7, 614−621

permittivity materials. *Physical Review Materials* **2019**, *3* (1), No. 015202.
(40) Dunkelberger, A. D.; Spann, B. T.; Fears, K. P.; Simpkins, B. S.; Owrutsky, J. C. Modified relaxation dynamics and coherent energy exchange in coupled vibration-cavity polaritons. *Nat. Commun.* **2016**, *7*, 13504.
(41) Shalabney, A.; George, J.; Hutchison, J.; Pupillo, G.; Genet, C.; Ebbesen, T. W. Coherent coupling of molecular resonators with a microcavity mode. *Nat. Commun.* **2015**, *6*, 5981.
(42) Simpkins, B. S.; Fears, K. P.; Dressick, W. J.; Spann, B. T.; Dunkelberger, A. D.; Owrutsky, J. C. Spanning Strong to Weak Normal Mode Coupling between Vibrational and Fabry−Pérot Cavity Modes through Tuning of Vibrational Absorption Strength. *ACS Photonics* **2015**, *2* (10), 1460−1467.
(43) Ismail, N.; Kores, C. C.; Geskus, D.; Pollnau, M. Fabry-Perot resonator: spectral line shapes, generic and related Airy distributions, linewidths, finesses, and performance at low or frequency-dependent reflectivity. *Opt. Express* **2016**, *24* (15), 16366−16389.
(44) Yee, H. Y.; Felsen, L. B.; Keller, J. B. Ray Theory of Reflection from the Open End of a Waveguide. *SIAM J. Appl. Math.* **1968**, *16* (2), 268−300.
(45) Luna, L. E.; Tadjer, M. J.; Anderson, T. J.; Imhoff, E. A.; Hobart, K. D.; Kub, F. J. Dry Etching of High Aspect Ratio 4H-SiC Microstructures. *ECS J. Solid State Sci. Technol.* **2017**, *6* (4), P207−P210.
(46) Paarmann, A.; Razdolski, I.; Gewinner, S.; Schöllkopf, W.; Wolf, M. Effects of crystal anisotropy on optical phonon resonances in midinfrared second harmonic response of SiC. *Phys. Rev. B: Condens. Matter Mater. Phys.* **2016**, *94* (13), 134312.

https://dx.doi.org/10.1021/acsphotonics.0c00071
ACS Photonics 2020, 7, 614−621